J Appl Electrochem (2009) 39:1779–1787
DOI 10.1007/s10800-009-9877-3

ORIGINAL PAPER

Development of composite anode electrocatalyst for direct methanol fuel cells

Xiaoxia Li · Xinping Qiu · Long Zhao · Liquan Chen · Wentao Zhu

Received: 10 February 2008 / Accepted: 17 March 2009 / Published online: 9 April 2009

Abstract Different effects of support hydrophilicity and metal-oxide on the performance of Pt-based catalysts were investigated with the aim of improving the mass activities toward methanol electrooxidation. Both potentiodynamic and potentiostatic measurements revealed that improved surface hydrophilicity of multi-wall carbon nanotubes (MWCNTs) could promote the dispersion of Pt nanoparticles and, consequently, promote the Pt utilization and reduce the polarization in methanol electrooxidation. In addition, WO_3 was shown to play a supportive role in enhancing catalytic activity. The interaction between Pt and WO_3 was examined by CO-stripping and CO oxidation transient experiments. The results suggested that the activity and the kinetics of monolayer CO_{ads} electrooxidation of Pt nanoparticles are enhanced by the adjacent WO_3 via a bifunctional mechanism, which accounts for improved activity in methanol electrooxidation.

Keywords Methanol electrooxidation · CO electrooxidation · Surface hydrophilicity · WO_3 · Direct methanol fuel cells

1 Introduction

Recently, direct methanol fuel cells (DMFCs) have emerged as promising power sources [1, 2]. However, the application of DMFCs is restricted by two critical drawbacks in conventional anodic catalysts of carbon supported Pt (Pt/C), including the high cost and the sluggish kinetics of methanol electrooxidation at low temperatures [2–4]. With regard to carbon supported anodic catalysts, there are several factors that greatly influence reaction activities and kinetics, such as the nature of the support, the Pt particle size and the catalyst composition [5–9]. Carbon nanotubes (CNTs), as a representative of one-dimensional carbon materials, have been studied extensively as the catalyst support to generate a porous catalytic layer and improve their performance [10, 11]. Furthermore, surface modification of carbon support has been shown to have a positive impact on catalytic performance. The results of Wang et al. [12] showed that O_3 treatment could improve the surface hydrophilicity of carbon black as well as the dispersion of Pt particles, and therefore promoted proton transport and methanol electrooxidation. Han et al. [13] pointed out that a pre-treated CNT surface had more sites for Pt particle anchoring as the concentration of nitric acid in the surface modification was increased. The resulting high performance of the catalysts was due to the high homogeneity of Pt particles on the support.

It is well known that the intermediate CO-like species can poison the active Pt sites and impair the kinetics of methanol electrooxidation. Transition-metal oxides, including $RuO_2 \cdot xH_2O$ [4], TiO_2 [14, 15], CeO_2 [16], MoO_x [17] and SnO_2 [18], increase the CO-tolerance of Pt particles and reduce the cost as a co-catalyst. Among them, WO_3 has been shown by different groups to have beneficial effects on the performance of Pt particles but with different explanations. Yang et al. [19] pointed out that WO_3 improved the performance of Pt and PtRu particles via promoting the dispersion of metal particles on the support rather than via a real catalytic mechanism. The work of Park's group [20, 21] showed that WO_3 promoted Pt catalytic properties via the "H-spillover" effect. However, the

X. Li · X. Qiu (✉) · L. Zhao · L. Chen · W. Zhu
Key Laboratory of Organic Optoelectronics and Molecular Engineering, Department of Chemistry, Tsinghua University, Beijing 100084, China
e-mail: Qiuxp@mail.tsinghua.edu.cn

experiments of Maillard et al. [22] focused on its role in CO electrooxidation. Their results showed that WO_3 enhanced Pt catalytic performance via the bifunctional mechanism. Given these various interpretations, the beneficial role of WO_3 in the kinetics of CO electrooxidation still needs further investigation to develop an in-depth understanding of the interactions between Pt and WO_3.

In our approach, microwave radiation was applied to modify the carbon surface with less time and more efficiency. The dependence of catalytic performance on surface modification was investigated by dynamic cyclic voltammetry, steady-state chronoamperometry and polarization curves. In addition, the interaction between Pt and WO_3 was studied and is discussed comparatively via CO-stripping and CO oxidation transient experiments.

2 Experimental

2.1 Preparation and characterization of the catalysts

Multi-wall carbon nanotubes (provided by theDepartment of Chemical Engineering, Tsinghua University) were treated by two methods after being ultrasonically radiated for 1 h. In the first method, 1.0 g of MWCNTs were refluxed in HCl aqueous solution (120 mL, 2 mol L^{-1}) at 80 °C for 48 h under stirring, then rinsed and dried according to the procedure reported [4], and denoted as $MWCNT_a$. In the second method, 1.0 g of MWCNTs were microwave-treated [23] in a mixed solution of 18 mol L^{-1} H_2SO_4/12 mol L^{-1} HNO_3 (0.1 L/0.1 L) for 3 min in air (for safety reasons, the microwave oven was placed in a fume hood and the treatment carefully conducted), rinsed thoroughly with deionized water, dried at 70 °C for 12 h, and denoted as $MWCNT_{ao}$.

Pure Pt catalysts supported on different MWCNTs were prepared with a one-step polyol process [24]. Typically, 0.0800 g of $MWCNT_a$ or $MWCNT_{ao}$ was ultrasonically treated in 120 mL ethylene glycol for 1 h; a calculated amount of hexachloroplatinic acid (dissolved in ethylene glycol) was added dropwise and the mixture was refluxed at 130 °C for 3 h under stirring. After being filtrated, rinsed and dried, the catalysts $Pt/MWCNT_a$ or $Pt/MWCNT_{ao}$ were prepared. The composite catalyst (with the addition of WO_3) was prepared by two steps. Firstly, 0.0800 g of $MWCNT_{ao}$ was ultrasonically dispersed in HCl aqueous solution (500 mL, 0.5 mol L^{-1}) for 1 h, followed by dropwise adding 3.2 mmol L^{-1} Na_2WO_4 aqueous solutions under continuous stirring to obtain Precursor 1. Then Precursor 1 was treated at 400 °C for 4 h in a flow of N_2 to form Precursor 2. Secondly, a nominal 20 wt% Pt was deposited on precursor 2 as H_2PtCl_6 and reduced by $NaBH_4$ [19] to fabricate the composite catalyst $Pt–WO_3/MWCNT_{ao}$.

The X-ray powder diffraction (XRD) patterns of the products were investigated via a Bruker powder diffraction system (model D8 Advanced) using CuKα as the radiation source (operating voltage: 40 kV, scan rate: 6° min^{-1}). The average size of Pt particles was calculated from the diffraction peak of Pt (220) (scan rate: 1° min^{-1}, 2θ range: 61–74°) using the Debye-Scherrer formula [25]. The surface morphology of the products was observed using transmission electron microscopy (TEM, JEOL model JEM-2010) at 120 kV. The catalyst composition was investigated by energy dispersive X-ray spectrometry (EDS, Oxford Instrument) plus scanning electron microscopy (SEM, LEO-1530) at 10 kV. In EDS investigations, at least 2 measurements were conducted for each sample to calculate the average value. Typically, an area of ca. 1 μm × 1 μm was scanned for at least 200 s to control the quantitative error to a minor level.

2.2 Electrochemical assessment

A square piece of gold foil (1 cm × 1 cm) coated by catalyst ink was used as the working electrode. The ink was prepared by ultrasonically dispersing the catalyst in a mixture of deionized water and Nafion solution (Nafion:ethylene glycol=1:4, v:v) for 30 min. Then the ink was cast onto the gold foil and air-dried at 80 °C for 1 h to form the working electrode. The gold foil was tested and showed no activity for the methanol and CO electrooxidation reactions.

Electrochemical measurements were conducted on a potentiostat (EG&G Princeton, PAR 273A) at 25 °C. A Pt foil (1 cm × 1 cm) and a saturated calomel electrode (SCE) were used as the counter and reference electrodes, respectively. In a conventional three-electrode cell, the reference electrode was placed in a separate chamber, located near the working electrode through a Luggin capillary tube. All potentials presented in this study are referred to SCE.

To estimate the electro-activity of the catalysts, cyclic voltammetry (CV) experiments were performed in the potential range −0.2 to +1.0 V in the electrolyte of 1 mol L^{-1} $HClO_4$ + 1 mol L^{-1} CH_3OH at a scan rate of 50 mV s^{-1}. Typically, constant current was reached after several cycles. The anodic peak current (forward sweep, at 0.75 V) of the 50th cycle was used to calculate the mass activity (normalized by the weight of Pt, mA mg^{-1} Pt) for comparison. The chronoamperometric tests for methanol oxidation were conducted for 3,600 s at a fixed potential of 0.45 V.

The in situ oxidation of pre-adsorbed CO was examined by CO stripping. The corrected charge of CO-stripping curves was used to calculate the electroactive surface area (*ESA*, m^2 g^{-1}) [26, 27]. Initially, N_2 gas was purged into

the electrolyte for 10 min. Then, CO gas was bubbled for 20 min to allow adsorption of CO onto the electrocatalyst at 0 V vs. SCE, then the dissolved CO was removed by bubbling N_2 into the electrolyte for 20 min, meanwhile, maintaining the potential at 0 V. Finally, the CO-stripping voltammogram was collected between −0.2 and 1.0 V at a scan rate of 20 mV s^{-1}. The curves of CO oxidation transients were collected after the same CO adsorption procedure, as the potential was stepped from 0 V to 0.4 V or 0.45 V, respectively.

3 Results and discussion

3.1 Physicochemical characterization of the as-prepared catalysts

By EDS investigation, the Pt content was tested to be 15.2 wt%, 22.5 wt%, and 20.6 wt% for Pt/$MWCNT_a$, Pt/$MWCNT_{ao}$, and Pt–WO_3/$MWCNT_{ao}$, respectively. The content of WO_3 in Pt–WO_3/$MWCNT_{ao}$ catalyst was found to be 1.7 wt%. The measurement of Pt–WO_3/$MWCNT_{ao}$ was taken as an example and is demonstrated in Fig. 1.

X-ray diffraction was used to trace the formation of WO_3 on $MWCNT_{ao}$. Figure 2 shows the XRD patterns of Precursor 1, Precursor 2 and the product Pt–WO_3/$MWCNT_{ao}$. The diffraction peaks at ~26.1° and 42.6° (labelled with the asterisks) in all of the patterns are the representative peak (002) and (100) of graphite, which demonstrate that the crystalline nature of MWCNTs is not destroyed during the pretreatment [5]. Except for the diffraction patterns of graphite, the pattern in Fig. 2a is nearly identical to the standard values (JCPDS-ICDD File No. 18-1418), which can be readily indexed to the phase of $WO_3 \cdot H_2O$, indicating that the reaction of Eq. 1 occurred during the preparing procedure.

$$Na_2WO_4 + 2HCl \rightarrow WO_3 \cdot H_2O + 2NaCl \quad (1)$$

Differing from Fig. 2a, the intensity of typical peak (020) for $WO_3 \cdot H_2O$ (Fig. 2b) decreases significantly along with the appearance of the diffraction pattern of WO_3 (JCPDS-ICDD File No. 43-1035), suggesting that the dehydration of $WO_3 \cdot H_2O$ occurred at 400 °C and formed WO_3 phase [28].

The diffraction peaks (020)/(200) and (202)/(220) of WO_3 were maintained in the sample of Pt–WO_3/$MWCNT_{ao}$ after Pt deposition, as displayed in Fig. 2c. The low intensity of WO_3 peaks arises from its low content in the catalysts. Meanwhile, the typical peak (020) of $WO_3 \cdot H_2O$ disappears completely, which might be due to its dissolution during the process of Pt deposition. Typical diffraction peaks (111), (200), (220), and (311) of Pt at 2θ values of 39.8°, 46.2°, 67.5°, and 81.4° (marked by #) are observed, indicating the face-centered cubic (fcc) structure of the Pt formed. The peak intensities are similar to the standard values, suggesting there is no priority orientation in the Pt crystal growth. The similar pattern of Pt/$MWCNT_a$ and Pt/$MWCNT_{ao}$ are not shown for clarity. According to the broadening peaks of

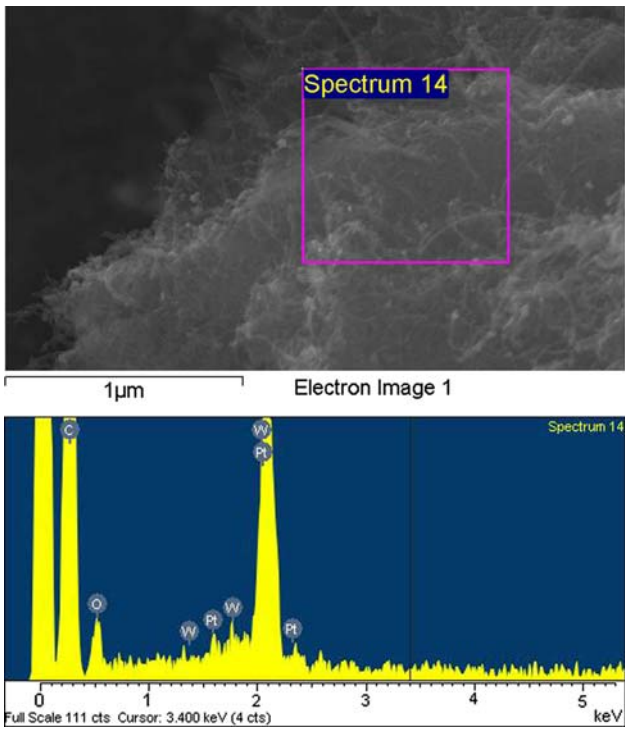

Fig. 1 Typical SEM image (*top*) and the corresponding EDS pattern (*bottom*) of the as-prepared Pt–WO_3/$MWCNT_{ao}$

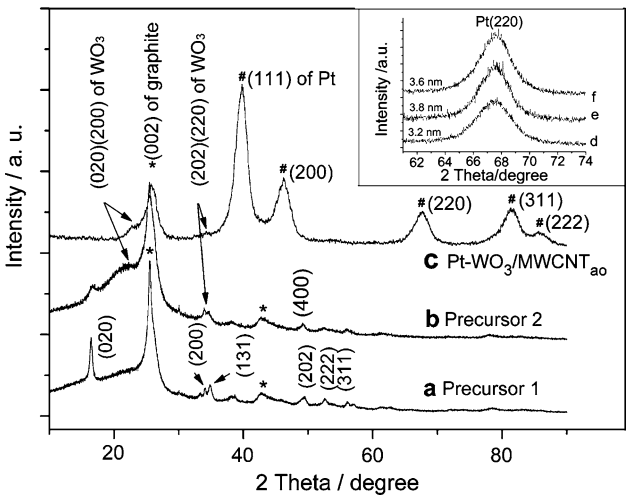

Fig. 2 Typical XRD patterns of (a) Precursor 1, (b) Precursor 2 and (c) the product Pt–WO_3/$MWCNT_{ao}$. The peaks located near 26.1° and 42.6° (marked with asterisk) are the representative peak (002) and (100) of graphite. The patterns of Pt (220) in the inset for sample (d) Pt/$MWCNT_a$ (e) Pt/$MWCNT_{ao}$ (f) Pt–WO_3/$MWCNT_{ao}$ are used to calculate the mean size of Pt particles

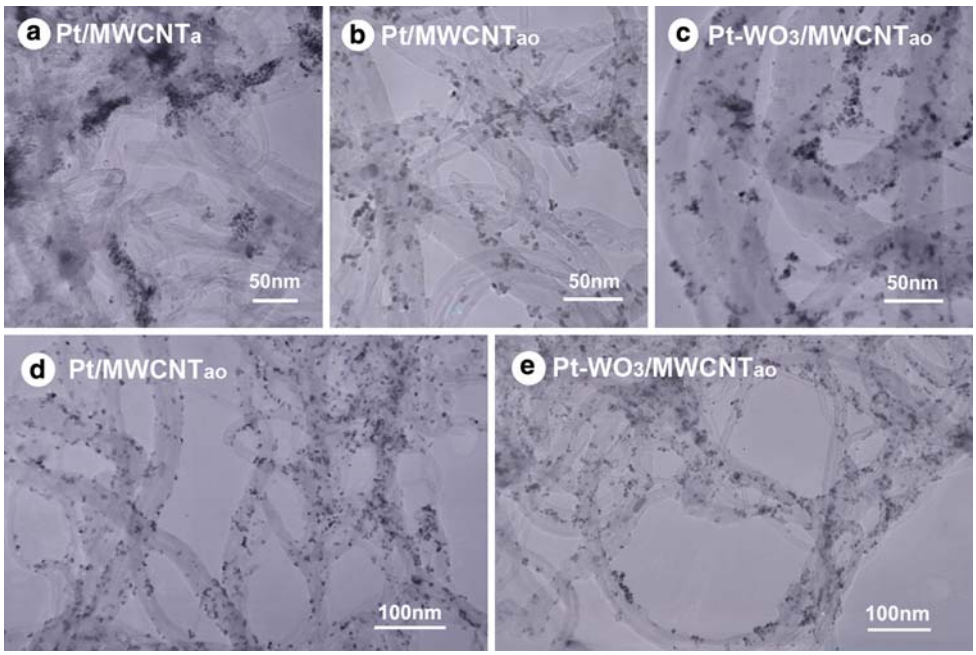

Fig. 3 Typical TEM images (*top*) at high magnifications for the as-prepared (**a**) Pt/$MWCNT_a$, (**b**) Pt/$MWCNT_{ao}$, (**c**) Pt–WO_3/$MWCNT_{ao}$; and the overall view images (*bottom*) for the two latter samples (**d**) Pt/$MWCNT_{ao}$ and (**e**) Pt–WO_3/$MWCNT_{ao}$ at relative low magnifications

(220), displayed in the inset of Fig. 2, the mean size of Pt particles for Pt/$MWCNT_a$, Pt/$MWCNT_{ao}$, and Pt–WO_3/$MWCNT_{ao}$ are calculated to be 3.2 nm, 3.8 nm and 3.6 nm, respectively.

Typical TEM images of the three catalysts are shown in Fig. 3 at different magnifications. From the top three images (Fig. 3a–c) at high magnification, spherical-shaped Pt particles are observed with narrow size distribution for the three samples. However, their dispersion differed significantly. Pt nanoparticles load (Fig. 3a) passively on $MWCNT_a$ with a strong tendency to agglomerate, resulting in inhomogeneous dispersion. Major parts of $MWCNT_a$ have no Pt particles on their surface. In contrast, Pt particles are observed to anchor on $MWCNT_{ao}$ in a more homogeneous manner in Fig. 3b and c. In order to illustrate this difference, the typical overall views of two latter samples were displayed at a relative low magnification in Fig. 3d and e, respectively. It is clear that Pt particles disperse in a widespread uniform manner for the $MWCNT_{ao}$ supported samples. The polarized surfaces of $MWCNT_{ao}$ seem to have more sites to deposit Pt. Possible reasons are discussed in the following Raman measurements. However, WO_3 cannot be discerned from Fig. 3c, possibly due to its low content and similar contrast to carbon. To further examine the dispersion of WO_3, EDS elemental mapping was performed for the elements Pt, W, O, and C, respectively. Figure 4a is a typical TEM image for sample Pt–WO_3/$MWCNT_{ao}$, and the Panels (b–e) are

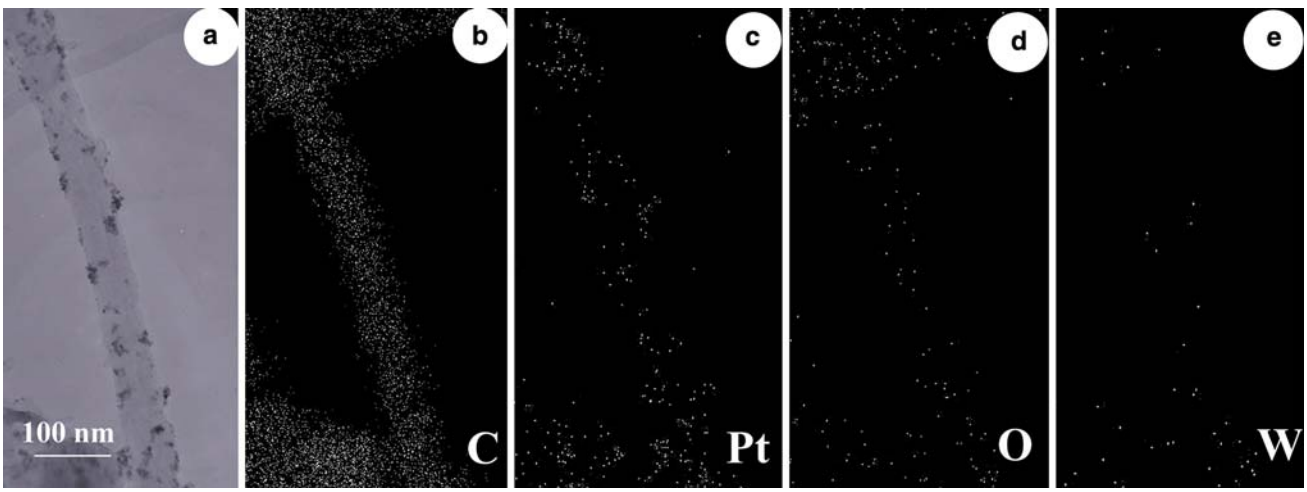

Fig. 4 **a** TEM image for the sample of Pt–WO_3/$MWCNT_{ao}$, and **b–e** the corresponding EDS elemental mapping for the image in **a**

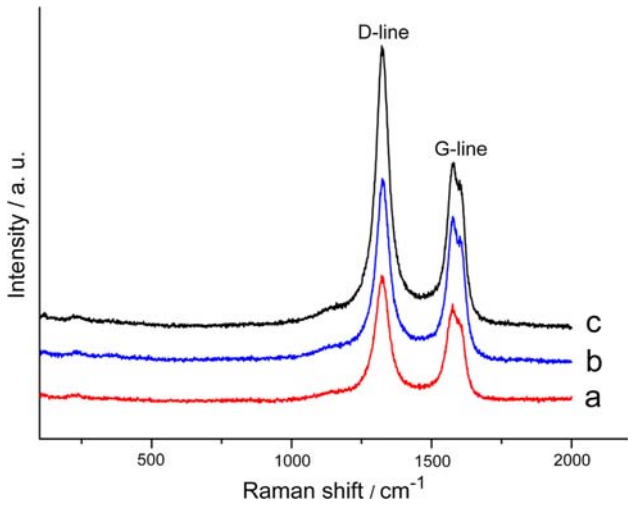

Fig. 5 Raman spectra of (a) as-received MWCNTs, (b) $MWCNT_a$, and (c) $MWCNT_{ao}$

its different elemental mappings. Both Pt and WO_3 are found on the surfaces of $MWCNT_{ao}$. However, the distribution of WO_3 is not uniform.

As mentioned above, distinct dispersion of Pt particles was observed on different modified surfaces. To examine the possible reasons, Raman spectra were recorded to probe surface structure of MWCNTs, as shown in Fig. 5. Noticeably, all the spectra have a similar pattern but present different intensity ratios. The absorption band observed at 1,573 cm^{-1} (G-line) corresponds to the Raman-allowed E_{2g} stretching mode of graphite, which reflects the structural intensity of the sp^2-hybridized carbon atoms. The band at 1,327 cm^{-1} (D-line) is a disorder-induced peak, which may originate from the structure defects of MWCNTs [5, 29]. Thus the extent of the defect in MWCNTs can be evaluated by the intensity ratio of the D- and G-lines (I_D/I_G). The I_D/I_G ratios for the pristine MWCNTs, the as-obtained $MWCNT_a$, and $MWCNT_{ao}$ are calculated to be 1.29, 1.27, and 1.72, respectively. The value of $MWCNT_{ao}$ is higher than that of the former two, suggesting more defects have formed on their surfaces. These defects could be due to the formation of oxygen-rich groups on their sidewalls during the microwave radiation in the H_2SO_4–HNO_3 mixture. More defects were reported to improve their surface hydrophilicity and dispersion in aqueous solution [23]. The dispersion of Pt particles increased along with more defects formed on the support surface, indicating the defects were advantageous to Pt deposition. This explains the high-homogeneity of Pt nanoparticles on the surface of $MWCNT_{ao}$.

3.2 Electrochemical characterization of the as-prepared catalysts

The catalyst activity towards methanol electrooxidation was investigated by cyclic voltammetry, as presented in Fig. 6. The performance of benchmark Pt/C (E-Tek, 20 wt% Pt, supported by carbon black) was studied for comparison. The mass activities of the catalysts at 0.75 V were found in an increasing order: the benchmark Pt/C $\sim$ $Pt/MWCNT_a$ $\ll$ $Pt/MWCNT_{ao}$ $<$ $Pt–WO_3/MWCNT_{ao}$. An increase of

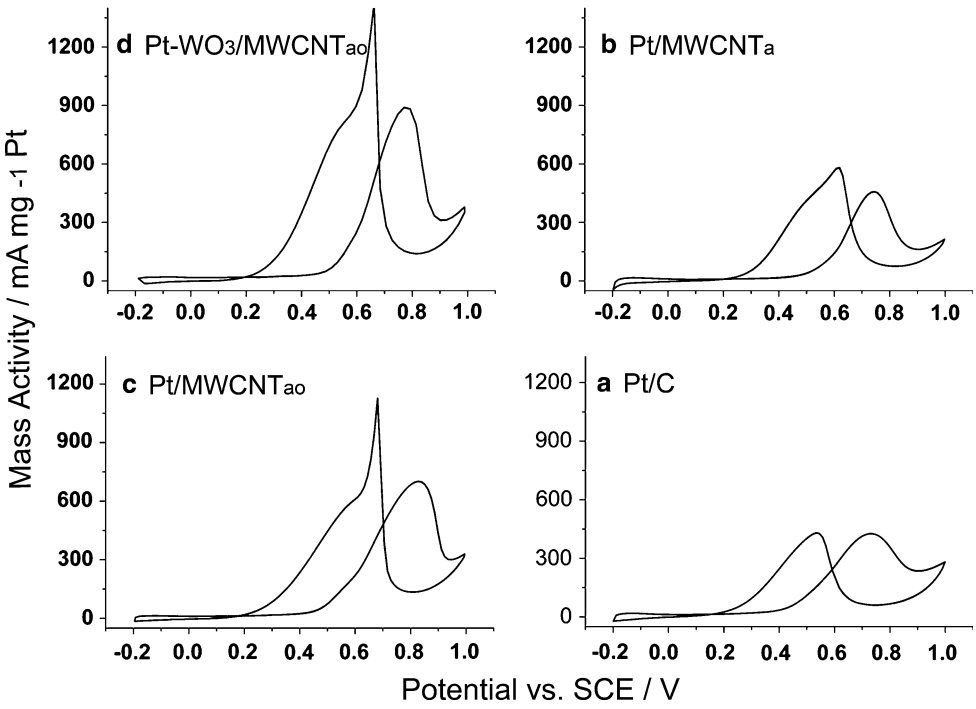

Fig. 6 Cyclic voltammetry curves of **a** the benchmark Pt/C, **b** $Pt/MWCNT_a$, **c** $Pt/MWCNT_{ao}$, **d** $Pt–WO_3/MWCNT_{ao}$, only the 50th cycle ones are demonstrated for clarity (in the electrolyte of 1 M $HClO_4$ + 1 M CH_3OH solution, 50 mV s^{-1}, 25 °C)

~97% and ~56% was found for Pt–WO_3/$MWCNT_{ao}$ (ca. 885 mA mg^{-1} Pt) and Pt/$MWCNT_{ao}$ (ca. 700 mA mg^{-1} Pt) as compared to the values for Pt/$MWCNT_a$ or benchmark Pt/C (ca. 450 mA mg^{-1} Pt), respectively. Noticeably, the value for benchmark Pt/C was in line with our previous values [4, 15]. Considering the similar particle size of Pt and distinct dispersion of Pt for the three samples, we can conclude that the remarkably improved activity was caused by the improved Pt dispersion rather than the particle size.

Apart from the results of Raman analysis, the improved hydrophilicity was also directly presented by the precipitation experiments, as depicted in Fig. 7. The time required to precipitate the ultrasonically dispersed Pt/$MWCNT_a$ was 5 h (Fig. 7-2a), which was much shorter than that for the $MWCNT_{ao}$ supported samples (Fig. 7-2b and 2c). The aforementioned oxygen-rich groups formed on the surfaces of $MWCNT_{ao}$ are polarized ones, which have a positive interaction with solvent molecules in aqueous solution and prevent them from bunching together. In contrast, the non-polarized surfaces of $MWCNT_a$ have a strong tendency to curve together in aqueous solution and result in a faster precipitation. The enhanced hydrophilicity was also helpful in fabricating a more uniform porous catalyst layer for the working electrode of the $MWCNT_{ao}$ supported catalysts with the same loading (Fig. 7-3).

The values of Pt utilization can help us understand the beneficial effect of the improved hydrophilicity. In order to compare the utilization of Pt particles, we calculate the real surface area of Pt (S_R) according to the following [30],

$$S_R = 6 \times 10^3 / \rho d;$$

supposing that the Pt particles are spherical with a uniform diameter (d), where ρ=21.4 g cm^{-3} is the density of the Pt metal and d is calculated from the XRD patterns. As listed in Table 1, the utilization of Pt is defined as the ratio of the electroactive surface area ESA to the real surface area S_R. The values of the $MWCNT_{ao}$ supported catalysts is found to be 20–25% higher than that of the $MWCNT_a$ supported one; meanwhile, the values for the two $MWCNT_{ao}$ supported samples are similar. This may be attributed to the higher dispersion of Pt particles and their better contact with the electrolyte on the polarized support surface. As a result, the mass activities of sample Pt–$MWCNT_{ao}$ and Pt–WO_3/$MWCNT_{ao}$ are enhanced. However, the increased percentages of Pt utilization are lower than the increased percentages of mass activities. This may possibly be ascribed to some other beneficial reasons, which are unknown at this stage.

Except for the dynamic CV investigation, steady-state chronoamperometry was applied to study the activities and catalyst poisoning in methanol electrooxidation from another aspect. Figure 8 shows that time transient curves (recorded at 0.45 V vs. SCE) are similar for the three

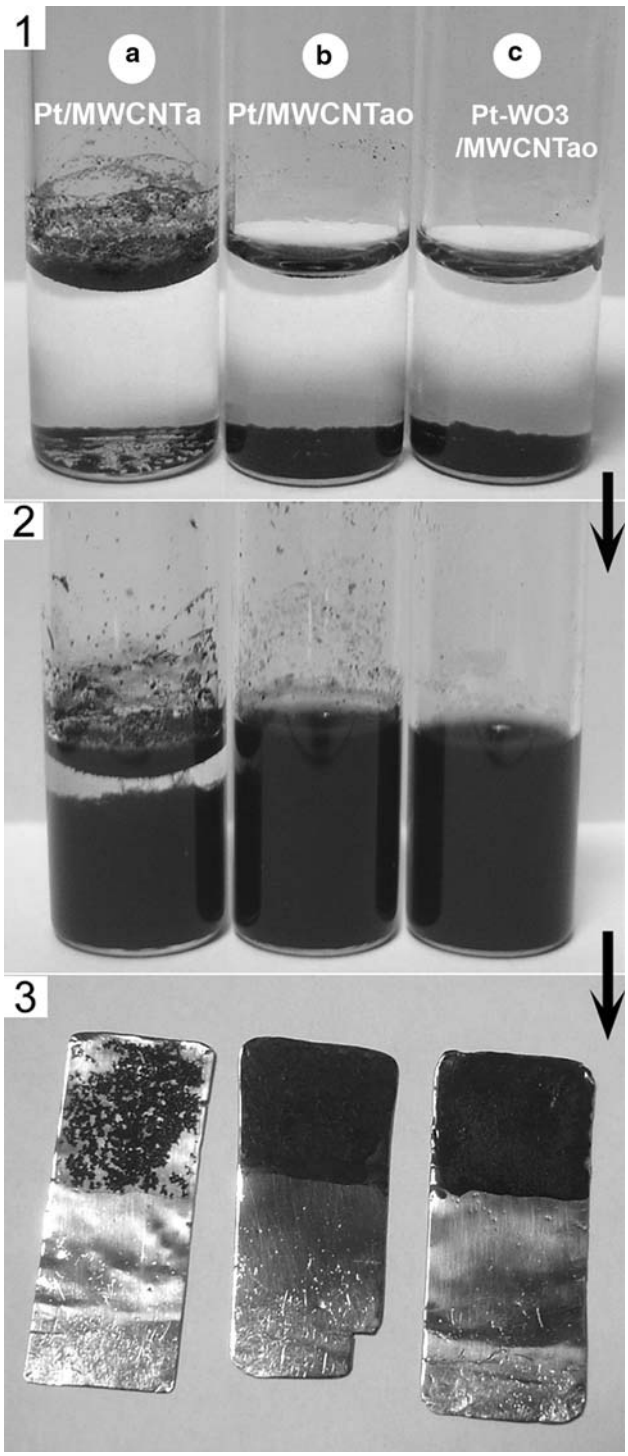

Fig. 7 Photographs of 2 mg of catalysts (a) Pt/$MWCNT_a$, (b) Pt/$MWCNT_{ao}$ and (c) Pt–WO_3/$MWCNT_{ao}$ in 3 mL deionized water, taken (**1**) before ultrasonic dispersion, (**2**) at the 5th hour after ultrasonic treatment for 30 min, and (**3**) photographs of fabricated working electrodes for ~0.6 mg of catalyst a, b, and c

catalysts. The specific current decreased rapidly at the beginning, perhaps due to the accumulation of intermediate CO-like species adsorbed on Pt active sites during the

Table 1 Comparison of the measured electroactive surface area, the calculated real surface area, and the utilization of Pt particles for the as-prepared catalysts

Catalyst	Pt–$MWCNT_a$	Pt/$MWCNT_{ao}$	Pt–WO_3/$MWCNT_{ao}$
ESA ($m^2\ g^{-1}$)[a]	41.7	43.9	44.3
D (nm)	3.2	3.8	3.6
S_R ($m^2\ g^{-1}$)	87.6	73.8	77.9
Pt utilization (%)[b]	47.6	59.5	56.9

[a] The values were measured in the next part of CO-stripping experiments

[b] Pt utilization (%) = $ESA/S_R \times 100\%$

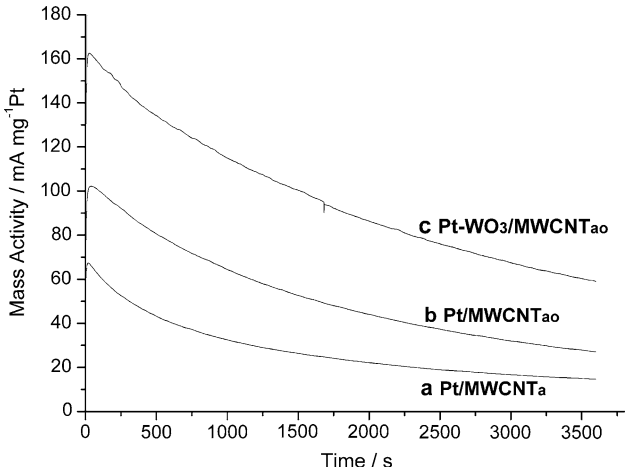

Fig. 8 The chronoamperometric curves for the catalysts (a) Pt/$MWCNT_a$, (b) Pt/$MWCNT_{ao}$ and (c) Pt–WO_3/$MWCNT_{ao}$, recorded at the oxidation potential of 0.45 V vs. SCE for 3,600 s in the electrolyte of 1 M $HClO_4$ + 1 M CH_3OH solution, 25 °C

methanol oxidation reactions [31]. After a long time of operation, the current decay slowed. This is attributable to a gradually developed semi-equilibrium between the poisoning and the activation process. The mass activities for Pt–WO_3/$MWCNT_{ao}$ are found to be the highest in the whole process, while the values for Pt/$MWCNT_a$ are the lowest. The results indicate the highest activity of Pt–WO_3/$MWCNT_{ao}$ in static measurements, which is consistent with the CV conclusions.

Furthermore, overall polarization performance on the three electrodes was investigated by a series of potentiostatic tests in the whole potential range of 0.2–0.6 V for 1,800 s, as plotted in Fig. 9. To reach the same mass activity in the same electrolyte, electrode Pt–WO_3/$MWCNT_{ao}$ needs the lowest overpotential; meanwhile Pt/$MWCNT_a$ needs the highest one and the value for Pt/$MWCNT_{ao}$ falls in between. This shows that reaction polarization on the three electrodes decreases in the sequence Pt/$MWCNT_a$ > Pt/$MWCNT_{ao}$ > Pt–WO_3/$MWCNT_{ao}$. Noticeably, the polarization on the anode of Pt–WO_3/$MWCNT_{ao}$ is not increased although the

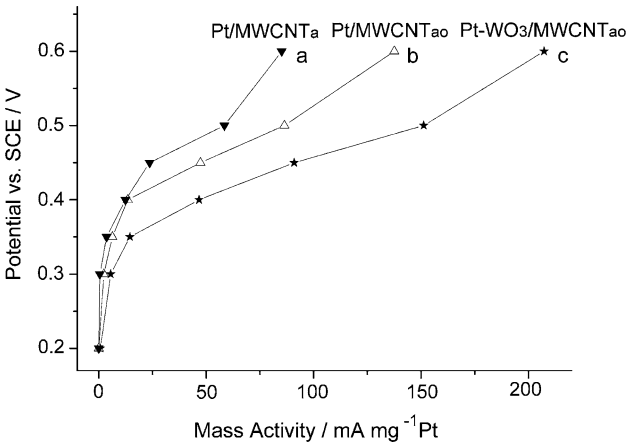

Fig. 9 The potentiostatic polarization profiles for the electrode of (a) Pt/$MWCNT_a$, (b) Pt/$MWCNT_{ao}$ and (c) Pt–WO_3/$MWCNT_{ao}$ were examined in the electrolyte of 1.0 M $HClO_4$ + 1.0 M CH_3OH at 25 °C

addition of the semiconductor WO_3 would decrease its electronic conduction. This can be ascribed to the low content of WO_3. $MWCNT_{ao}$ with high hydrophilicity is beneficial in improving the Pt utilization as well as forming a uniform layer structure, which favors high catalytic efficiency and, consequently, reduces the surface reaction polarization.

It is clear that the results of steady-state measurements are in line with those of dynamic CV. The performance of Pt–WO_3/$MWCNT_{ao}$ was observed to be better than Pt/$MWCNT_{ao}$, indicating that the WO_3 concomitance might be the reason for the improved activities. CO-stripping and CO oxidation transients were conducted to study the role played by WO_3. Figure 10 compares the shape and peak potential (E_p) of CO-stripping curves for the three catalysts. All curves were recorded under similar catalyst

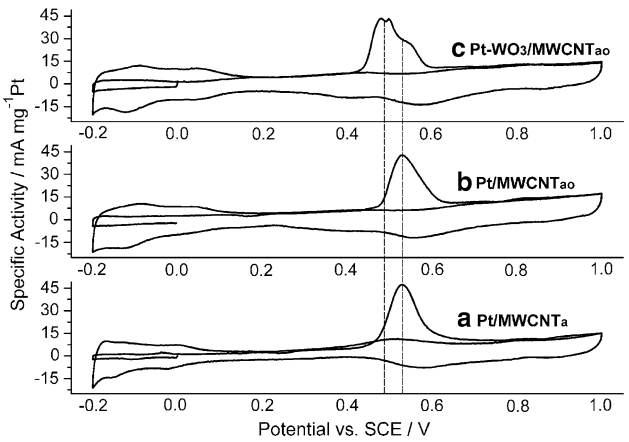

Fig. 10 CO-stripping curves of (**a**) Pt/$MWCNT_a$, (**b**) Pt/$MWCNT_{ao}$ and (**c**) Pt–WO_3/$MWCNT_{ao}$, investigated in 1 mol L^{-1} $HClO_4$ solution, 20 mV s^{-1}, 25 °C

loading (ca. 0.5 g cm^{-2}). Only one peak was found for both Pt/MWCNT$_a$ and Pt/MWCNT$_{ao}$ with the same potential $E_p = 0.53$ V. The E_p for benchmark Pt/C was found at a higher position of 0.59 V (not shown for clarity), which was in line with the literature value [4]. In the case of the composite Pt–WO_3/MWCNT$_{ao}$, however, the shape and E_p are quite different from that of pure Pt catalyst. A new strong peak (E_p at ca. 0.48 V) was discernible, which accompanies the peak of $E_p = 0.53$ V. In the literature, peak multiplicity in CO-stripping curves has been ascribed to CO electrooxidation on different parts (terraces and edges) [32] or different crystallographic orientations [33] of Pt. However, these explanations cannot be applied to spherical Pt particles without any priority orientation in our experiments. Considering that the peak $E_p = 0.53$ V is at the exact same position as that of pure Pt catalysts, we propose that there are two different forms of Pt particles presenting in Pt–WO_3/MWCNT$_{ao}$ catalyst: the particles deposited far away from WO_3 and the particles adjacent to WO_3. This is readily understood due to the un-homogenous dispersion of WO_3 and its low content. Unlike the electronic interaction between Pt and the second metal (such as Ru, Sn) in the alloy catalysts, WO_3 has little influence on the electronic density of adjacent Pt particles. WO_3 was reported [22] to improve the catalytic activity of Pt particles through the well-accepted bifunctional mechanism in acid media by providing more oxygen-rich species to assist water dissociation. Since CO_{ads} surface diffusion can hardly spillover the carbon substrate [22], only the Pt particles adjacent to WO_3 have enhanced activity to oxidize CO with a negative E_p shift from 0.53 V to 0.48 V. In contrast, the particles deposited alone on the surface of MWCNT$_{ao}$ are in the same chemical circumstance as pure Pt catalysts and keep their inherent position of $E_p = 0.53$ V. Remarkably, the onset potential of Pt–WO_3/MWCNT$_{ao}$ is 0.44 V, which is also lower than that of pure Pt catalysts (0.48 V). Given the lower onset and peak potential in CO electrooxidation, the electrode of Pt–WO_3/MWCNT$_{ao}$ presented a rational higher activity than that of Pt/MWCNT$_{ao}$ towards methanol electrooxidation.

The peak multiplicity in CO-stripping curves was proposed to originate from the existence of two forms of Pt nanoparticles. This matches well with the results of Maillard et al. [22], in that better CO-tolerance would be achieved when the interaction between Pt and WO_3 is maximized. However, the peak multiplicity is quite different from the results of Yang et al. [19], in which the presence of WO_3 in $PtWO_x$/C and $PtRuWO_x$/C catalysts was supposed to result in some physical modification rather than a true catalytic mechanism. In addition to the results of CO-stripping, the role of WO_3 was further investigated using CO oxidation transients at two fixed potentials, as demonstrated in Fig. 11. At 0.45 V, the time required to reach the maximum current

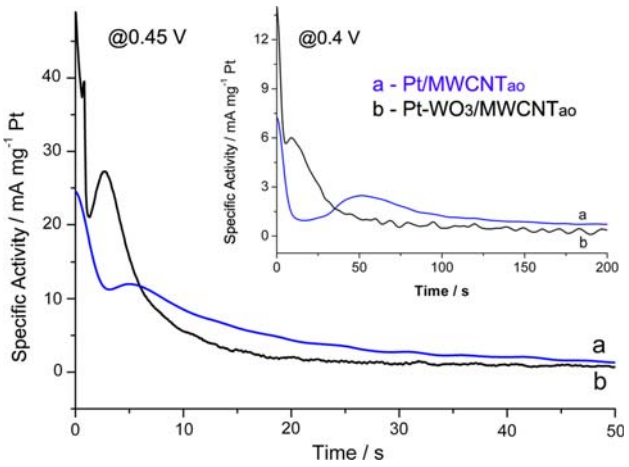

Fig. 11 The curves of CO oxidation transients at the electrode of (a) Pt/MWCNT$_{ao}$ and (b) Pt–WO_3/MWCNT$_{ao}$ were recorded as the potential stepped from 0 V to 0.45 V vs. SCE. The inset curves were recorded as the potential stepped from 0 V to 0.4 V vs. SCE

(t_0) for CO oxidative removal is 2.5 s for catalyst WO_3–Pt/MWCNT$_{ao}$, which is much shorter than the time of 5 s for Pt/MWCNT$_{ao}$. The difference is magnified at the lower potential of 0.40 V (displayed in the inset), as t_0 is 9 s for the former and 51 s for the latter. Small t_0 for CO oxidation is found for WO_3–Pt/MWCNT$_{ao}$ at two potentials, suggesting faster kinetics for CO oxidative removal [6] in the presence of WO_3. This is in good agreement with the results for CO-stripping. Evidently the combined results of CO-stripping and CO oxidation transients display a co-catalyst role of WO_3 in CO electrooxidation, which accounts for the high activities of catalyst WO_3–Pt/MWCNT$_{ao}$ towards methanol electrooxidation.

In addition, the *ESA* of Pt were calculated to be 41.7, 43.9, and 44.3 m^2 g^{-1} for Pt/MWCNT$_a$, Pt/MWCNT$_{ao}$, and Pt–WO_3/MWCNT$_{ao}$ from the corrected CO-stripping charge. To subtract the influence of *ESA* on the activity towards methanol electrooxidation, we obtained the specific activity for the three catalysts by normalizing the mass activity with *ESA*. The values were calculated to be 1.08, 1.59 and 2.00 mA cm^{-2} Pt for Pt/MWCNT$_a$, Pt/MWCNT$_{ao}$, and Pt–WO_3/MWCNT$_{ao}$, respectively. This suggests clearly that the improved activities for Pt–WO_3/MWCNT$_{ao}$ are due to the combined effects of the enhanced hydrophilicity and the co-catalyst effect of WO_3.

The observed beneficial role of WO_3 revealed that the interaction between Pt and WO_3 could increase the kinetics of CO electrooxidation and the activity of methanol electrooxidation, which was assumed to perform via the bi-functional mechanism. However, the possible origin of such a result is still incompletely understood. The discussion is beyond the scope of our experiments, which require more in situ studies or theoretical calculations. The performance comparison between PtW alloy and Pt–WO_3

composite catalysts could be another way to help obtain a greater depth of understanding.

4 Conclusions

The composite catalyst Pt–WO_3/$MWCNT_{ao}$ was found to have higher performance than Pt/$MWCNT_{ao}$, Pt/$MWCNT_a$, and the benchmark Pt/C catalyst towards methanol electrooxidation. The improved activity was ascribed to two effects: the improved hydrophilicity of the support and the assistance of WO_3. Both potentiodynamic and potentiostatic results showed that the enhanced surface hydrophilicity of $MWCNT_{ao}$ greatly improved Pt utilization, and consequently promoted the mass activities as well as decreasing the anodic polarization. Furthermore, WO_3 was shown to promote CO electrooxidation via the interaction with adjacent Pt, examined by CO-stripping and CO oxidation transients. Low onset and peak potentials were observed in CO-stripping for the catalyst Pt–WO_3/$MWCNT_{ao}$ in comparison to catalyst Pt/$MWCNT_{ao}$; the time required to reach the maximum current for CO oxidative removal for the former was less at the two fixed potentials in CO oxidation transients. The results of CO-stripping and CO oxidation transients were in good agreement, which suggested that the activity and the kinetics of CO_{ads} monolayer electrooxidation of Pt nanoparticles were promoted by the adjacent WO_3. The assistance of WO_3 also accounted for its high activity in methanol electrooxidation.

Acknowledgements Financial support of this work by the State Key Basic Research Program of PRC (2002CB211803), Natural Science Foundation of Beijing (2051001), and the China Postdoctoral Science foundation (20060400459) is gratefully acknowledged.

References

1. Liang HP, Zhang HM, Hu JS et al (2004) Angew Chem Int Ed 43:1540
2. Liu HS, Song CJ, Zhang L et al (2006) J Power Sources 155:95
3. Ganesan R, Lee JS (2005) Angew Chem Int Ed 44:6557
4. Cao L, Scheiba F, Roth C et al (2006) Angew Chem Int Ed 45:5315
5. Tian ZQ, Jiang SP, Liang YM et al (2006) J Phys Chem B 110:5343
6. Maillard F, Eikerling M, Cherstiouk OV et al (2004) Faraday Discuss 125:357
7. Arenz M, Mayrhofer KJJ, Stamenkovic V et al (2005) J Am Chem Soc 127:6819
8. Park SH, Xie Y, Weaver MJ (2002) Langmuir 18:5792
9. Gasteiger HA, Markovic N, Ross PN et al (1994) J Phys Chem 98:617
10. Kongkanand A, Vinodgopal K, Kuwabata S et al (2006) J Phys Chem B 110:16185
11. Liu ZL, Lin XH, Lee JY et al (2002) Langmuir 18:4054
12. Wang ZB, Yin GP, Shi PF (2006) Carbon 44:133
13. Han KI, Lee JS, Park SO et al (2004) Electrochim Acta 50:791
14. Tian J, Sun GQ, Jiang LH et al (2007) Electrochem Commun 9:563
15. Song HQ, Qiu XP, Li FS et al (2007) Electrochem Commun 9:1416
16. Wang JS, Xi JY, Bai YX et al (2007) J Power Sources 164:555
17. Ioroi T, Yasuda K, Siroma Z et al (2005) J Electrochem Soc 150:A1225
18. Ke K, Waki K (2007) J Electrochem Soc 154:A207
19. Yang LX, Bock C, MacDougall B et al (2004) J Appl Electrochem 34:427
20. Park KW, Ahn KS, Choi JH et al (2002) Appl Phys Lett 81:907
21. Park KW, Ahn KS, Choi JH et al (2003) Appl Phys Lett 82:1090
22. Maillard F, Peyrelade E, Soldo-Olivier Y et al (2007) Electrochim Acta 52:1958
23. Wang YB, Iqbal Z, Mitra S (2006) J Am Chem Soc 128:95
24. Zhou ZH, Wang SL, Zhou WJ et al (2003) Chem Commun 3:394
25. Radmilovic V, Gasteiger HA, Ross PN (1995) J Catal 154:98
26. Bock C, MacDougall B (2003) J Electrochem Soc 150:E377
27. Scheiba F, Scholz M, Cao L et al (2006) Fuel Cells 06:439
28. Nogueira HIS, Cavaleiro AMV, Rocha J et al (2004) Mater Res Bull 39:683
29. Li W, Bai Y, Zhang YK et al (2005) Synth Met 155:509
30. Yang RZ, Qiu XP, Zhang HR et al (2005) Carbon 43:11
31. Kabbabi A, Faure R, Durand R et al (1998) J Electroanal Chem 444:41
32. Guerin S, Hayden BE, Lee CE et al (2004) J Comb Chem 6:149
33. Solla-Gullon J, Vidal-Iglesias FJ, Herrero E et al (2006) Electrochem Commun 8:189